Biosensors and Bioelectronics 123 (2019) 237–243

Contents lists available at ScienceDirect

Biosensors and Bioelectronics

journal homepage: www.elsevier.com/locate/bios

Improved microfluidic platform for simultaneous multiple drug screening towards personalized treatment

Oihane Mitxelena-Iribarren[a,b,*], Jon Zabalo[b], Sergio Arana[a,b], Maite Mujika[a,b]

[a] Ceit, Manuel Lardizábal 15, 20018 Donostia / San Sebastián, Spain
[b] Universidad de Navarra, Tecnun, Manuel Lardizábal 13, 20018 Donostia/San Sebastián, Spain

ARTICLE INFO

Keywords:
Microfluidics
Microstructure
Drug screening
Cancer therapy
Personalized treatment

ABSTRACT

Development of new targeted therapies is a challenge in the battle against cancer. Although a variety of treatments is currently available, there is no technique for rapidly evaluating the response of cancer patients to the drug. In this work, a microfluidic platform for the real-time simultaneous analysis of the success rate of different nanoparticle based chemotherapeutic drugs is presented. Based on a previous planar chamber and a reported sensitivity enhancing strategy, linear and cross shape microstructures were integrated into the chamber dome of the microfluidic polydimethylsiloxane and glass platform in order to provide a higher fluid mixing and treatment-cell interaction. Several methotrexate (MTX) based treatments (free MTX, MTX loaded Lecithin-PVA nanoparticles, MTX loaded Lecithin-Tween 80 nanoparticles) as well as their respective controls (cell media and both blank nanoparticles) were recirculated through the microchamber over an osteosarcoma cell monolayer. These nanovehicles reduced cell population to less than 20% (LEC-PVA nanoparticles) and 2.3% (LEC-Tween nanoparticles), demonstrating that nanoparticles are a promising target therapy for cancer treatment. Moreover, microstructured platforms demonstrated a higher efficacy in the drug-screening process: due to the liquid folding a higher amount of nanoparticles was internalized by the cells and, therefore, results were observed faster. In fact, the time required to reduce cell viability to the half was nearly a 75% faster. Furthermore, this microfluidic platform offers the capability to test up to five different drugs simultaneously, making it a powerful tool to evaluate the effect of multiple drugs and determine the most effective and personalized treatment.

1. Introduction

Cancer is one of the main mortality causes all over the world (World Health Organization, 2018). More specifically, it is the second main cause of death in the European Union and in the United States (Ferlay et al., 2013). It was estimated by the year 2050, 27 million of new cancer cases will be diagnosed, among which 17.5 million will die. Many of the first line therapies used nowadays against cancer involve surgery, with or without previous chemotherapy, followed by chemotherapy and radiation (Yamamoto and Tsuchiya, 2013). Nevertheless, these treatments demonstrated having several side effects. Chemotherapeutic treatments also take a long time to show progress (Hassan et al., 2010; Kuczynski et al., 2013). In addition, cancer can even keep growing due to the development of resistance to the chemotherapeutic agents (Yang et al., 2014). Moreover, some chemodrugs get disposed indiscriminately increasing the morbidity of the patients and causing certain temporary side effects, such as hair loss (Hanahan and Weinberg, 2000). All these undesired effects are related to the limited specificity and lack of targeting capability over cancer cells. Therefore, there is a need for improvement and personalization of cancer therapy.

In recent years, novel therapies were developed in order to offer an efficient and targeted treatment avoiding unnecessary damage to healthy tissue. On the one side, targeted therapy takes advantage of the higher vascular permeability of tumors. On the other side, it uses different stimuli or substances to identify and attack cancer cells in a more precise and effective way, usually causing less damage to healthy tissue (Sanna et al., 2014). This principle of action decreases the toxicity associated with the conventional treatments. Among all the nanosystems, the use of nanoparticles was reported as a promising strategy in cancer treatment (Hu et al., 2010). These vehicles are nanometric size particles with a diameter between approximately 50 and 100 nm (Battaglia et al., 2014) and are composed of biodegradable and biocompatible lipids. They can carry the drug located in the particle core (Soares et al., 2014), in the shell (Rostami et al., 2014) or dispersed within the whole lipid matrix (Shi et al., 2014). It was demonstrated that lipid

* Corresponding author at: Ceit, Manuel Lardizábal 15, 20018 Donostia / San Sebastián, Spain.
E-mail address: omitxelena@ceit.es (O. Mitxelena-Iribarren).

https://doi.org/10.1016/j.bios.2018.09.001
Received 20 August 2018; Accepted 1 September 2018
Available online 02 September 2018
0956-5663/

nanoparticles can act as therapeutic vehicles for antineoplastic drugs or that they can be orally administered (Das and Chaudhury, 2011; Pathak and Raghuvanshi, 2015). Due to their improved pharmacokinetic profiles, permeability and retention effect and increased drug accumulation at tumor sites, they present less side effects than other therapies (Davis et al., 2008; Matsumura and Maeda, 1986; Peer et al., 2007).

While lipid nanoparticle delivery provided new hope for cancer treatment, methodological issues slowed down their application. Usually, in vitro testing of these vehicles is performed using traditional techniques (such as well-plates) that do not fully replicate the tumor microenvironment (Pandya et al., 2017). However, these offer a limited potential due to fluid stagnation and possible nanoparticle sedimentation, which could hide the real effects of the vehicles. These limitations, together with the fact that rapid screening techniques to evaluate the efficacy of anti-cancer drugs are needed in the timely management of cancer (Morabito et al., 2014), make personalized cancer therapies to require new methods for efficient drug screening.

The use of microfluidics in the biomedical field demonstrated to be a powerful platform to monitor the response of cancer cells to different drugs, to develop alternative technologies for dynamic biomedical applications or for cancer research (Bhise et al., 2014; Boussommier-Calleja et al., 2016; Mitxelena-Iribarren et al., 2017; Pavesi et al., 2016; Riahi et al., 2015; Streets and Huang, 2014). Microfluidic platforms were presented as a powerful alternative in vitro system for nanoparticle-cell interaction analysis (Farokhzad et al., 2005). Biological systems are characterized for micrometric structures and well-controlled fluid flows. Both aspects, together with the manipulation of small sample volumes and processes, can be controlled in microfluidic platforms, as they have sizes similar to the biological length scales. Microfluidic devices offer highly-controlled fluidics, channel geometry and microenvironment control and the real-time monitoring of the process inside the device (Liu et al., 2017). Microfluidics also provide with other advantages in biomedical applications, such as improved sensitivity over other techniques, time efficiency or reduced reagent and sample volumes even manipulating individual cells (Reece et al., 2016; Song et al., 2018). In addition, they also allow multi-parameter studies on cancer cells, providing rapid analysis of small amounts of patient derived cells (Mao and Huang, 2012). However, the characteristic pure laminar flow of microfluidic platforms prevents from a full interaction between the nanoparticles flowing in the circulating liquid and the cells located at the bottom part of the channel. In fact, only the particles in the lowest layers interact with the cells, while most of the therapeutic agent contained in the fluid does not contact them.

Several approaches to avert the laminar flow related to microfluidics can be found in the literature. One of the most effective strategies was proposed by Stroock *et al.* in 2002 (Stroock et al., 2002). This research group embedded microstructures in the bottom of a channel to create a 3D folding and mix the fluids at the microscale. Since then, this strategy was widely used for several applications such as increasing the target delivery to immunosensors (Golden et al., 2007), increasing the binding of proteins to their ligands (Foley et al., 2008) or the capture of circulating tumor cells (Stott et al., 2010). In all the cases, the use of microstructures enhanced the interaction between the desired particles.

Considering all the above mentioned facts, a microfluidic platform for the real-time simultaneous analysis of the success rate of nanoparticle based chemotherapeutic drugs is presented in this work. Based on a previously reported sensitivity enhancing strategy (Gomez-Aranzadi et al., 2015), linear and cross shape microstructures were integrated into the chamber dome of the microfluidic polydimethylsiloxane platform in order to provide a higher fluid mixing and treatment-cell interaction. Furthermore, this microfluidic platform offers the capability to test up to five different drugs simultaneously, favoring the rapid assessment of multiple drugs. After choosing the best nanoparticle mixing platform design, the new microfluidic device was evaluated using an osteosarcoma cell line treated under both free and encapsulated methotrexate (MTX), as well as their respective controls. Moreover, the cytotoxicity observed in the microstructure containing platform was validated by comparing it with a similar planar platform earlier described in the literature (Mitxelena-Iribarren et al., 2017).

The current series of experiments present a rapid, sensitive and effective toxicity platform to identify the effect of drugs on cancer. In order to optimize the design of the microstructure used to improve the microfluidic platform, 2D mixing assessment was performed by means of color mixing in PDMS-glass platforms. 3D mixing was determined using PDMS-silicon platforms. Finally, the cytotoxicity assays performed with the final PDMS-glass platforms demonstrated that these new devices provide an accurate, reliable and effective screening of new anti-cancer therapeutics, which entails a significant development towards personalized medicine.

2. Materials and methods

2.1. Design of microfluidic platforms

In this work different microfluidic platform prototypes were designed with CAD software (AutoCAD® 2015, Autodesk Inc.). Based on a previous plain microfluidic platform (Mitxelena-Iribarren et al., 2017), six different microstructures were embedded at the void of the microfluidic chamber. These structures are divided in two main groups according to their design: cross shape microstructures (two designs) and linear microstructures (4 designs). Designs of each group differ in the width of the microstructure (25 or 50 μm) and the separation between them (25 or 50 μm, only in the case of linear microstructures).

Moreover, the number of inlets of the referenced platform was modified, increasing the main treatment inlet from one to three or five inlets. This provided the opportunity to introduce different treatments simultaneously.

2.2. Fabrication and characterization of microfluidic platforms

The six prototypes, together with the plain design, were fabricated in two different ways: in polydimethylsiloxane (PDMS, Silastic T4, Dow Corning) and silicon (for the fluorescent nanoparticle assay) and in PDMS and glass (for the velocity, color mixing and cytotoxicity assays).

The fabrication of PDMS-glass platforms was performed following previously described procedures (Gomez-Aranzadi et al., 2015). In summary, in order to obtain the microfluidic platform, PDMS replica-molding techniques were performed, using molds fabricated by double layer UV lithography on 4″ silicon wafers with SU-8 100 and SU-8 2015 negative photoresists (MicroChem Corp., USA). The first layer of the mold delimited the area of the microdevice (microchamber and microchannels), while the second layer defined the embedded microstructures. Then, once the PDMS was demolded, an oxygen plasma treatment was used to make the glass and PDMS surface hydrophilic. The plasma treatment provided a strong and irreversible bonding between them. This way the glass became the surface were cells were attached in the cytotoxicity assays and leaking was avoided in all experiments.

On the other hand, PDMS-silicon devices were fabricated using 4″ oxidized silicon wafers (Telecom-STC Co. Ltd., Russia) as the base substrate. The sensing areas were fabricated onto the silicon employing standard microsystem processes. The interaction with the metallized area was based on the attachment of an amine-sensitive molecular layer that could bind amine-coated nanospheres (Gomez-Aranzadi et al., 2015). Therefore, gold was chosen as the sensing surface due to its high affinity to the thiol (-SH) head groups of the 3-mercaptopropionic acid (MPA) used for the self-assembled monolayer (SAM). For that, a 150 nm thick gold layer was deposited and patterned through a lift-off process with conventional photolithography (using the Microposit S1818 positive photoresist purchased from Rohm and Haas Electronic Materials, LLC) and RF sputtering (Edwards ESM-100) methods. The sensing area comprised the whole microchamber and microchannel area. Once the

silicon piece was fabricated and the PDMS was demolded, plasma treatment was applied to both parts. In this case, the bonding was reversible, so that after the experimental procedures images of both components could be taken.

Both the molds, the PDMS replicas and the gold layer heights were characterized using a P-6 profilometer from Tencor-KLA Corporation (U.S.A.).

2.3. Cell culture and reagents

Firstly, experimental procedures to choose the best microstructures were carried out. In the color mixing experiments, different color dyes were employed. In the fluorescence experiments though, a self-assembled monolayer was created 3-mercaptopropionic acid (MPA),1-Ethyl-3-(3-dimethylaminopropyl) carbodiimide (EDC) and N-Hydroxysuccinimide (NHS), purchased from Thermo Scientific. Afterwards, 252 nm amine-coated fluorescent polystyrene spheres (Merck Chimie S.A.S., France) were circulated with an IPC Ismatec ISM937C peristaltic pump (IDEX Health & Science GmbH, Germany).

The U-2 OS (ECACC 92022711, ATCC HTB-96) osteosarcoma cell line was used for the velocity analysis and, once the microstructure was chosen, as a cancer model. Following the experimental procedure described elsewhere (Mitxelena-Iribarren et al., 2017), the cells were cultured using RPMI 1640 with Ultraglutamine 1 medium (RPMI 1640 with U1, Life Technologies, UK) supplemented with 10% (v/v) fetal bovine serum (FBS, Life Technologies, UK) and 1% of PenStrep (Gibco®, UK) at 37 °C in a humidified 5% CO_2 atmosphere. For subculturing, cells were washed with PBS, trypsinized with 0.5% trypsin-EDTA 1X (Gibco®, UK) and, once mixed with supplemented medium, centrifuged at 1500 rpm for 5 min. After this procedure, cells were used either for subculturing (performed three times a week using conventional protocols) or for velocity or cytotoxicity assays.

For cytotoxicity assays, both free and encapsulated methotrexate (MTX) was employed. Free MTX (kindly provided by Dr. A. Aldaz, from the Department of Pharmacy of Clínica Universidad de Navarra, Spain) was used as reference treatment to assess the effectiveness of the encapsulated MTX in two different concentrations: 15 μM and 150 μM. Two different lipid nanoparticles (kindly provided by Dr. MJ. Blanco, from the Faculty of Pharmacy of the University of Navarra) were analyzed in this study, named LEC-PVA and LEC-Tween. For both of them blank and MTX-loaded particles were used. Their fabrication was previously described by González-Fernández et al. (2015) and their manipulation was also reported earlier by this group (Mitxelena-Iribarren et al., 2017). The average size of the nanoparticles after resuspension in media was 281.7 ± 31.3 nm for the LEC-PVA and 158.9 ± 5.1 nm for the LEC-Tween. Corresponding PDI values were 0.257 and 0.365, respectively.

2.4. Experimental procedures

As mentioned before, three different experiments were performed to determine the effect that the microstructures had in the fluid flow inside the microchamber. For the final validation of the platform cytotoxicity assays was carried out afterwards.

In the first experimental procedure, cell velocity profiles inside the six different prototypes were measured, following the procedure described elsewhere (Mitxelena-Iribarren et al., 2017). Briefly, cells were inserted and circulated through the device using polymeric tubes of Tygon MHSL2001 with an internal diameter of 0.38 mm (Ismatec, Germany) and an Ismatec ISM597D peristaltic pump (IDEX Health & Science GmbH, Germany). The experiments were recorded with a Nikon D90 camera hitched to a Nikon Eclipse TS100 microscope and velocities of the cells were quantified with the "Cell Tracker" program extension of Matlab (The Mathworks, Inc). The maximum and non-zero minimum velocity values were obtained and then the velocity reduction factor was calculated for each microstructure configuration.

Secondly, the experiment named as the 2D color mixing assay was performed. With it, the diffusion at the color interphase was used to determine the in-plane mixing capacity of the different microstructures. In this case, multiple inlet platforms were used, in order to introduce 3 or 5 different colors at the same time. Once more, the flow was provided by the Ismatec ISM597D peristaltic pump and recorded with a Nikon D90 camera hitched to a Nikon Eclipse TS100 microscope. A sequencing of the image was then performed with Matlab, to determine the width of the interphases between the different colors. Briefly, a consecutive lecture of the pixel columns of the image covering all the color interphases was performed. These data were processed, obtaining the RGB code of each of the pixels contained in the columns to distinguish the interphases between the different colors (identified as the slopes) and the areas with "pure" colors (identified as the straight horizontal areas). After identifying the interphases, the width of each of them was quantified. In order to obtain a common term to compare the mixing ability of the different microstructures, the agitation factor was defined. The agitation factor is defined in this work as the percentage of the increase of the interphase between two colors in a platform containing microstructures in respect to the plain microfluidic platform. This agitation factor was calculated for each of the microstructures and a statistical analysis was performed to determine the effect of the microstructures in the color mixing.

The last experiment performed to analyze the 3D mixing effect of the microstructures was the fluorescence assay, the only experiment performed with the PDMS-silicon devices. In this case, the first step was to immobilize the SAM onto the patterned gold areas inside the finished devices. The composition and formation were prepared and characterized following previously described techniques (Gomez-Aranzadi et al., 2015; Zuzuarregui et al., 2014). During the process MPA diluted in ethanol was introduced into the microchannels, followed by an incubation period of 2 h. Afterwards, both EDC and NHS (diluted in deionized) water were sequentially circulated into the microdevices and let inside for an incubation period of 1 h each respectively. After the SAM formation, the amine-coated nanospheres (0.1 mg/mL concentration in deionized water) were circulated for two hours over the sensing area with a continuous flow rate of 100 μL/min. This procedure was key to evaluate the effectiveness of the microstructures at increasing the surface-sample interaction by enhancing out-of-plane mixing. This interaction was evaluated comparing the fluorescence of the different sensing areas, as the nanoparticles emitted fluorescence in the FITC range (495–519 nm). Fluorescence images of the silicon part of the device were taken at the end of the nanoparticle circulation step with the Nikon Eclipse Ti microscope. Image analysis was performed with the NIS-Elements software and ImageJ, calculating the amount of fluorescent pixels in each case. Results are presented as the percentage of relative amount of nanosphere binding detected in the sensing areas.

In the three cases, results were always compared to the velocity, mixing rate and fluorescence signal obtained in the plain platforms.

Finally, once the optimum microstructure was chosen, cytotoxicity studies were performed to validate the platform. These assays were carried out recirculating different anti-cancer treatments over osteosarcoma cells in a set-up including a transmission Nikon Eclipse Ti microscope, following the procedure described earlier in the literature (Mitxelena-Iribarren et al., 2017). Both free and encapsulated MTX (LEC-PVA and LEC-Tween lipid nanoparticles) in two different concentrations (15 μM and 150 μM) were tested inside the microfluidic platforms. Cell media and blank lipid nanoparticles of the two types were also recirculated over the cells in order to determine their normal proliferation under a dynamic flow condition and to obtain a nanoparticle control.

2.5. Statistical analysis

The velocity reduction values obtained in the cell velocity assays were statistically analyzed using Matlab. Results are shown as mean

value ± standard deviation from corresponding replicates per category, with $n = 3$, $n \geq 3$ or $n \geq 4$ depending on the assay (as indicated in the Results section). Data analysis was done performing independent student's *t*-test when comparing the different heights or its equivalent non-parametric test when the requirements were not fulfilled. Following the same procedure, statistical analysis was also performed to analyze the color mixing and the fluorescent nanoparticle binding.

In addition, the cytotoxicity effect was determined using Matlab. In this case, when comparing only two groups, independent student's *t*-test (or Mann-Whitney-*U* tests) was performed. One-way analysis of variance (ANOVA) followed by post-hoc Bonferroni's test or its non-parametric equivalent test (Kruskall-Wallis test) was performed when comparing more than two groups.

The statistical significance criterion was the same for the four analyses. Statistical difference was determined as not significant (p-value > 0.05), significant (0.01 < p-value < 0.05), very significant (0.001 < p-value < 0.01) or extremely significant (p-value < 0.001).

3. Results and discussion

3.1. Fabrication and characterization of microfluidic platforms

Fabricated PDMS pieces were characterized after demolding them and before bonding them to the silicon or glass surfaces. As an average, microchannels had a height of 107.22 ± 5.00 μm, while microstructures as a whole showed a height of 30.92 ± 2.95 μm. Therefore, due to the embedded microstructures, the chamber had some areas of around 75 μm height. Examples of the different microstructures embedded in the PDMS microchambers can be observed in Fig. 1.

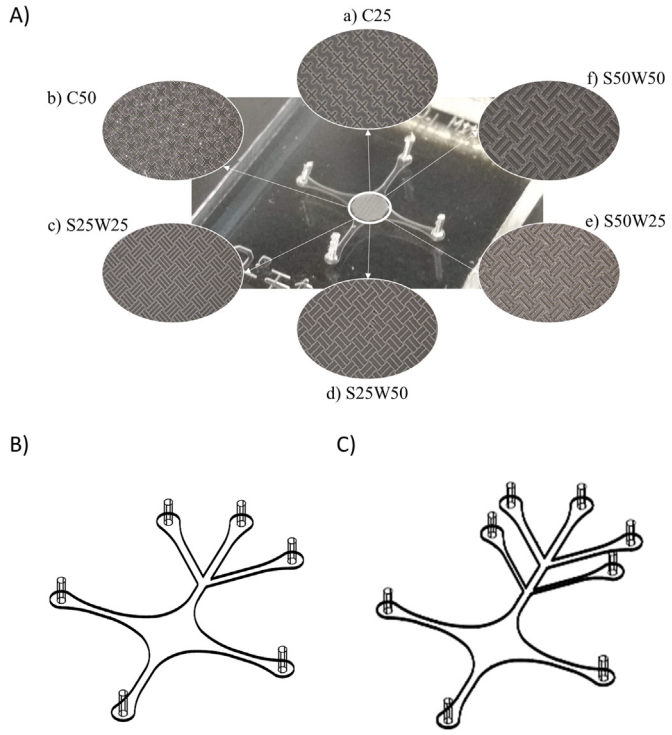

Fig. 1. A) Microstructured microfluidic platform in the center having the 1 inlet configuration as a base, with the six different designs of microstructures around it: a) cross shape microstructures of a width of 25 μm (C25); b) cross shape microstructures of a width of 50 μm (C50); c) linear microstructures of a width and separation of 25 μm (S25W25); d) linear microstructures of a width of 50 μm and separation of 25 μm (S50W25); e) linear microstructures of a width of 25 μm and separation of 50 μm (S25W50) and f) linear microstructures of a width and separation of 50 μm (S50W50). Schemes of the multiple-inlet microfluidic platforms with three (B) and five (C) inlets.

3.2. Velocity reduction assay

Experiments performed with the six platforms containing microstructures allowed for the estimation of the velocity of the cells while entering the microchambers. In previous studies, it was determined important to have the lowest nanoparticle velocity possible in the chamber to maximize the contact time between the circulating treatments and the adhered cells. However, it had to be ensured also that, in the case of nanovehicle based anti-cancer therapy, there was no nanoparticle sedimentation throughout the treatment. Therefore, as analyzed in previously published works (Mitxelena-Iribarren et al., 2017), the reduction from the maximum to the non-zero minimum velocity values were used to compare the influence of the integration of the microstructures to the top of the chamber.

The data analyzed with the Cell Tracker software allowed the calculation of the velocity reduction for each of the microstructure containing platforms. The data for the optimized plain platform was previously published (Mitxelena-Iribarren et al., 2017). In this work, this reduction of the velocity was considered as a reference to determine the effect of the microstructures could have in the nanoparticle velocity. The mean velocity reduction remained around the 810–870 μm/s in all the cases, which represents reduction of a 15–20%. The device with the linear microstructures of a width and separation of 25 μm (S25W25) was the one presenting the highest velocity reduction (Fig. 2). However, no statistically significant difference was observed when comparing the reduction of the velocities between all the microstructure-containing platforms and the plain one or between them.

However, it is remarkable that in all the platforms containing microstructures, the minimum velocity acquired was lower than the one obtained in the plain platforms, being between 77 ± 25 μm/s and 221 ± 33 μm/s for the microstructured platforms, and 290 ± 21 μm/s for the plain ones. This fact happens to be very convenient in this new anti-cancer drug testing platform, as more time for the nanoparticle-cell interaction would be allowed. Although statistical significance was not observed, the design with the lowest velocity (even lower than the one observed in the plain platform) was the S25W25 design.

3.3. Mixing efficiency of the microfluidic platforms

Once a proper velocity reduction was ensured with the microstructures, the mixing effectivity had to be quantified. This was performed with two different analyses: firstly, by quantifying the mixture of different color solutions inside the microfluidic PDMS-glass platform and then with fluorescence assays, analyzing the amount of amino-coated nanoparticles bond to the sensing area of the PDMS-silicon devices.

As mentioned earlier, different color solutions were circulated

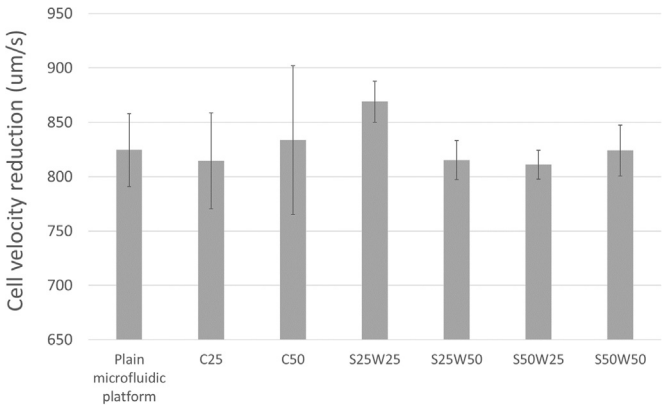

Fig. 2. Velocity reduction for each design (n ≥ 4). The obtained p-values for each comparison were all higher than 0.05, which show no significant difference between the microstructure containing and plain platforms.

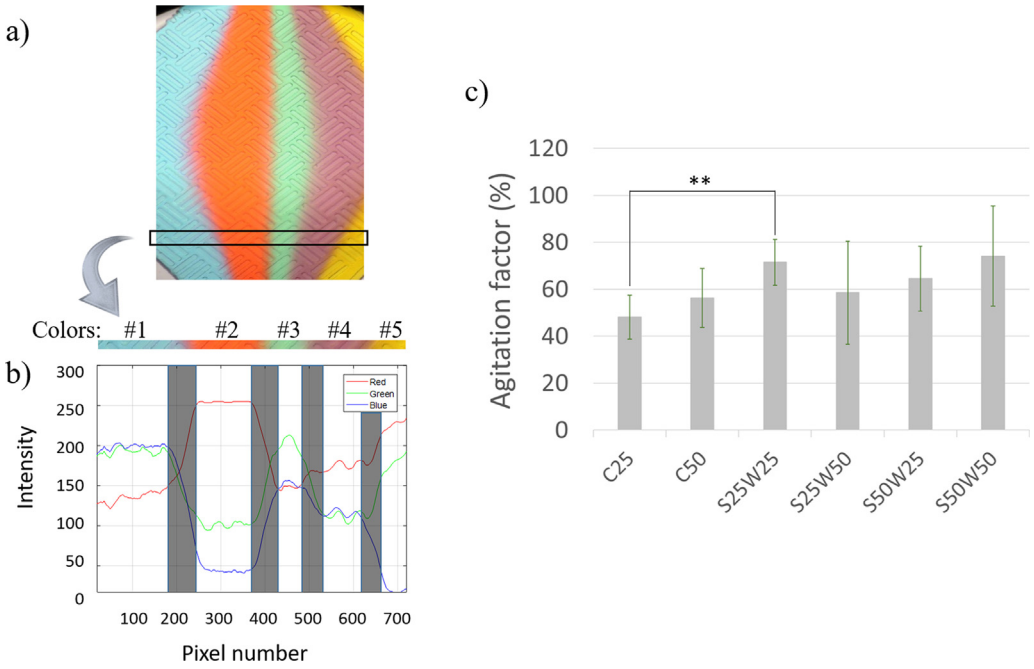

Fig. 3. a) Image of the color flows obtained with the Nikon D90 camera hitched to a Nikon Eclipse TS100 microscope, remarking the selection of a five-color pixel column as an example. b) Filtered RGB intensity graph of a column of pixels of a five color experiment. c) Percentage of the color interphase increase (agitation factor) of the microstructure containing platforms (n = 3). No significant difference was observed between the microstructure containing and the plain platforms (p-values > 0.05). Only the comparison C25 and S25W25 microstructures was statistically very significant (p-value = 0.002, **).

simultaneously inside the PDMS-glass platforms. According to the results obtained with the color image analysis (Fig. 3), all the platforms containing microstructures showed an agitation factor higher than 40%, demonstrating that any of the designs increases the two dimensional mixing of the flow. Although not significantly different from the others, the microstructures presenting the highest average values for the agitation factor were the linear microstructures of a width and separation of 25 μm (S25W25) and the linear microstructures of a width and separation of 50 μm (S50W50). A statistical analysis was performed to verify the significance of the two dimensional mixing. The analysis demonstrated a statistically significant difference with respect to the agitation obtained in the plain platforms (p-value < 0.05). Nevertheless, when comparing the effect of the different microstructures among them, only the comparison between the cross shaped microstructures of a 25 μm width (C25) and the S25W25 microstructures was statistically very significantly (p-value = 0.002).

Finally, fluorescence measurements were performed to analyze the mixing efficiency of the microfluidic platforms containing microstructures. After the SAM formation and the amino-coated nanoparticle circulation during two hours, images of the sensing area of the PDMS-silicon devices were taken with the Nikon Eclipse Ti microscope. An example of the images acquired is shown in Fig. 4. The image analysis performed with the silicon substrate of the different platforms provided the percentage of the chamber area covered by fluorescence, represented in the Fig. 4. Although there are small areas of fluorescence on the sensing areas of the plain microfluidic platforms, they are very dispersed and do not even reach the 1% of occupation, reflecting the low amount of nanoparticles reaching the SAM. Regions outside of the sensing areas do not display any nanoparticle attachment as expected, as no flow or SAM attachment with gold was in those areas. As observed in the graph, all the microstructures significantly enhanced the amino-coated nanoparticle binding to the surface. This enhancement tripled the binding achieved with the plain platforms. In fact, the difference in the fluorescence coverage was extremely significant for the G50 design (p-values = 0.0004) and significant for the rest of the designs (p-value < 0.04), with the exception of S50W50, which demonstrated no statistical difference with the plain platform. Specially, the S25W25 microstructures demonstrated a substantial increase, nearly 15 times more than the plain fluorescence signal, supporting the goal of increasing the sensitivity through the use of 3D flow within the

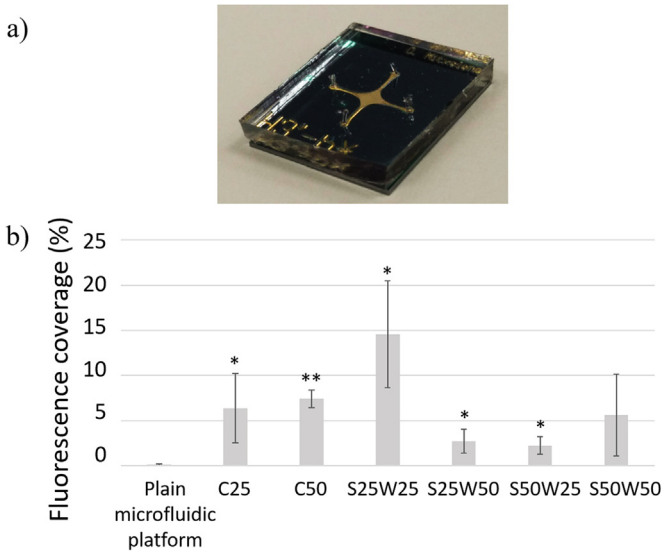

Fig. 4. a) Microstructured microfluidic platform fabricated in PDMS-silicon for the fluorescence assay. b) Quantification of the fluorescence of each device indicating the coverage percentage and the statistical significance in their comparison to the plain microfluidic platform (* is for 0.01 < p-value < 0.05 and ** for 0.01 < p-value < 0.001).

microfluidic device. Therefore, these experiments demonstrated that the integration of microstructures to the previously optimized microfluidic platform enhanced the vertical distribution of nanoparticles circulating along a microdevice, increasing the interaction of the flowing nanoparticles with the bottom of the device. As far as we know, this is the first time that this folding capacity is demonstrated in a chamber shape microspace, as all the related experiments were earlier performed in microchannels and not wider spaces with non-rectangular shapes.

Considering all the above mentioned results, the S25W25 microstructures were considered the best for the purpose of this work. Therefore, this platform was the one chosen to perform the cytotoxicity assay.

3.4. Cytotoxicity assay

As mentioned earlier, several methotrexate (MTX) based treatments (free MTX, MTX loaded Lecithin-PVA nanoparticles, MTX loaded Lecithin-Tween 80 nanoparticles) as well as their respective controls (cell media, blank Lecithin-PVA nanoparticles, blank Lecithin-Tween 80 nanoparticles) were recirculated through the microchamber over an osteosarcoma cell monolayer.

In order to assess the S25W25 microfluidic platform to quantify the cytotoxic effect of drug-loaded nanoparticles, cells were first subjected to regular cell media circulation assays. As demonstrated in earlier studies, cells proliferated and withstood damage caused by the continuous flow rate during the 72-h period. However, in this case, the rubbing induced by folding generated by the microstructures under the circulation rate of 2.15 μL/min did not let the cells grow as much as in the planar microfluidic platforms (up to 240% compared to 288%). This indicates a higher mechanical stress exerted on the cells due to a lower chamber height and the fluid mixing. Nevertheless, no cytostatic effect was observed since cells still continue growing under that flow.

Next, assays were performed to verify that inside the microdevices the increasing amount of MTX had an increasing cytotoxic effect. The two mentioned concentrations of the free drug (15 and 150 μM) were recirculated within the microstructure-containing platform. In this case, it can be inferred from the free MTX data that under the same drug concentration, cell population was slightly lower with the introduction of the microstructures than in the plain platforms. However, this difference was statistically not significant (p-values > 0.13), for any of the concentrations.

In the following step, lipid nanoparticles were recirculated over osteosarcoma cells. As described before, cells were subjected to blank lipid nanoparticles to assess the effect of adding a vehicle alone as a treatment, i.e. nanoparticle control. In this case, it was observed that cells did not grow as much as under cell media recirculation, confirming the same tendency observed in plain platforms. After checking that blank nanoparticles neither presented a cytotoxic effect in the microstructured platforms, drug-loaded nanoparticle assay was carried out. It was demonstrated once more that cell growth was significantly reduced under the recirculation of both types of drug-loaded nanoparticles compared to that with the free drug. Indeed, it was demonstrated that the efficiency of encapsulated methotrexate was much higher than that of the free methotrexate as the methotrexate containing nanoparticles had a higher cytotoxic effect. After 72 h of recirculation, these nanovehicles reduced cell population to less than 20% in the case of LEC-PVA nanoparticles and to a 2.3% in the case of LEC-Tween nanoparticles with a concentration of 15 μM inside the S25W25 microstructure containing platform. In the same period of time, cell viability was reduced to 0% when the concentration of both nanoparticles was increased to 150 μM, though. According to statistical analysis, the higher effect of the loaded lipid nanoparticles against osteosarcoma cells was statistically very significant compared to the free drug already after 12 h under MTX containing LEC-PVA and LEC-Tween nanoparticles (p-values = 0.03 and p-value = 0.006 respectively). This significance was observed even earlier in both cases when the concentration was increased to 150 μM.

In fact, the main advantage presented by these microstructure containing platforms was the quickness with which treatment effects were observed. Taking a look into the cell viability trend followed by both nanoparticle treatments in plain and S25W25 microfluidic platforms (Fig. 5), an extremely significant (p-value = 0.0007) and very significant difference (p-value = 0.003) was observed for MTX loaded LEC-PVA and LEC-Tween nanoparticles respectively just after 12 h of treatment recirculation. In both cases, when using the microstructure containing platforms, the effects of the nanoparticles are observed earlier than with the plain platforms. For example, when recirculation of LEC-Tween nanoparticles was performed, 48 h were required to see a cell viability of 60% in plain platforms, while this reduction was

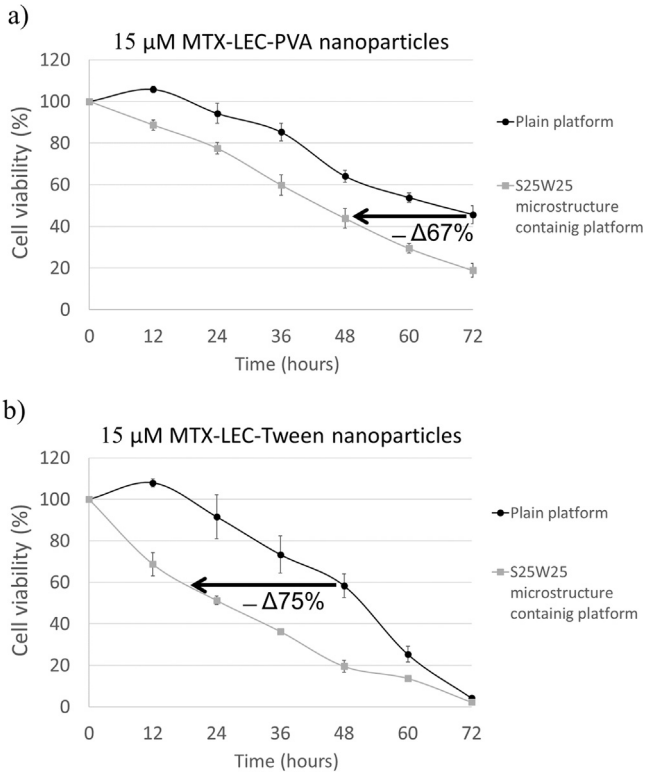

Fig. 5. a) Cell viability under 15 μM MTX- loaded LEC-PVA nanoparticle recirculation in plain and S25W25 microstructures containing microfluidic platforms (n ≥ 3); b) cell viability under 15 μM MTX- loaded LEC-Tween nanoparticle recirculation in plain and S25W25 microstructures containing microfluidic platforms (n ≥ 3). For both treatments, statistical significance (p-value < 0.003) was observed between the plain and S25W25 microstructured platforms already after 12 h.

observed after a bit more than 12 h with the microstructures. This demonstrates a reduction of the 75% of the time required to perform the study for these nanoparticles. Similarly, for LEC-PVA nanoparticles, the time required to see the same cytotoxic effect was also reduced, but not that abruptly. In this case, a cell viability a bit lower than the 50% was observed after 72 h in the plain platform, while in the microstructured one only 48 h had to pass (time reduction of 67%). This rapid effect of the nanoparticles observed in the new platforms is due to the liquid folding or mixing generated by the microstructures, which increases the amount of nanoparticles that reach the cell monolayer, and, therefore, increases the internalization and cytotoxicity. Thus, the effect of the nanoparticles is earlier observed with the use of microstructures in the analysis chamber area. This, together with the fact that the new microfluidic platforms offer the possibility to test up to 5 treatments at the same time, reduces the characterization and effectivity test of anticancer drugs from days to hours and, therefore, accelerates the choice of treatment for each patient improving the development of personalized medicine.

4. Conclusions

As a conclusion, based on a planar chamber and on a previously reported sensitivity enhancing strategy, linear and cross shape microstructures were integrated into the chamber-dome of the microfluidic PDMS and glass platform in order to provide a higher fluid mixing and treatment-cell interaction. Firstly, it was demonstrated that microstructures had the capacity to increase the mixing of the liquids, without disturbing the cell velocity reduction rates of the plain platforms. In fact, in the color mixing and fluorescence assays, the linear microstructures of a width and separation of 25 μm (S25W25) were

considered the best ones. They presented an agitation factor over 70% and their fluorescence coverage was 15 fold higher than the one in plain platforms. Once the microstructured platform was optimized, cytotoxicity studies were performed. The results obtained with the microstructured platforms confirmed that nanoparticles are a promising target therapy for cancer treatment, as MTX-loaded LEC-PVA nanoparticles reduced cell population to less than the 20% and MTX-loaded LEC-Tween nanoparticles to a 2.3% after 72 h of treatment recirculation. In both cases, it was demonstrated that the use of these nanovehicles was statistically significant in comparison to the treatment with the free drug. Moreover, microstructured platforms demonstrated this effectivity in a shorter time than the plain platforms, as the time required to reduce cell viability to the half was from 67–75% faster. In addition, this microfluidic platform offers the capability to test up to five different drugs simultaneously, making it a powerful tool to personally evaluate the effect of multiple drugs and determine the most effective treatment. Therefore, this platform could be used to rapidly test several drugs to choose the best treatment for each patient, improving their quality of life.

Data statement

The raw/processed data required to reproduce these findings cannot be shared at this time due to technical or time limitations.

Funding

This work was supported by the Spanish Association against Cancer (AECC) (convocatoria Cáncer Infantil 2014), Spain, and by the Basque Government (PREDOC program), Spain, financing Oihane Mitxelena's Ph.D. studies.

References

Battaglia, L., Gallarate, M., Panciani, P.P., Ugazio, E., Sapino, S., Peira, E., Chirio, D., 2014. Techniques for the preparation of solid lipid nano and microparticles. In: Application of Nanotechnology in Drug Delivery. InTech. https://doi.org/10.5772/58405.

Bhise, N.S., Ribas, J., Manoharan, V., Zhang, Y.S., Polini, A., Massa, S., Dokmeci, M.R., Khademhosseini, A., 2014. Organ-on-a-chip platforms for studying drug delivery systems. J. Control. Release 190, 82–93. https://doi.org/10.1016/j.jconrel.2014.05.004.

Boussommier-Calleja, A., Li, R., Chen, M.B., Wong, S.C., Kamm, R.D., 2016. Microfluidics: a new tool for modeling. Cancer. Interact. Trends Cancer 2, 6–19. https://doi.org/10.1016/j.trecan.2015.12.003.

Das, S., Chaudhury, A., 2011. Recent advances in lipid nanoparticle formulations with solid matrix for oral drug delivery. AAPS PharmSciTech 12, 62–76. https://doi.org/10.1208/s12249-010-9563-0.

Davis, M.E., Chen, Z.G., Shin, D.M., 2008. Nanoparticle therapeutics: an emerging treatment modality for cancer. Nat. Rev. Drug Discov. 7, 771–782. https://doi.org/10.1038/nrd2614.

Farokhzad, O.C., Khademhosseini, A., Jon, S., Hermmann, A., Cheng, J., Chin, C., Kiselyuk, A., Teply, B., Eng, G., Langer, R., 2005. Microfluidic system for studying the interaction of nanoparticles and microparticles with cells. Anal. Chem. 77, 5453–5459. https://doi.org/10.1021/ac050312q.

Ferlay, J., Steliarova-Foucher, E., Lortet-Tieulent, J., Rosso, S., Coebergh, J.W.W., Comber, H., Forman, D., Bray, F., 2013. Cancer incidence and mortality patterns in Europe: estimates for 40 countries in 2012. Eur. J. Cancer 49, 1374–1403. https://doi.org/10.1016/j.ejca.2012.12.027.

Foley, J.O., Mashadi-Hossein, A., Fu, E., Finlayson, B.A., Yager, P., 2008. Experimental and model investigation of the time-dependent 2-dimensional distribution of binding in a herringbone microchannel. Lab Chip. https://doi.org/10.1039/b713644g.

Golden, J.P., Floyd-Smith, T.M., Mott, D.R., Ligler, F.S., 2007. Target delivery in a microfluidic immunosensor. Biosens. Bioelectron. 22, 2763–2767. https://doi.org/10.1016/J.BIOS.2006.12.017.

Gomez-Aranzadi, M., Arana, S., Mujika, M., Hansford, D., 2015. Integrated microstructures to improve surface-sample interaction in planar biosensors. IEEE Sens. J. 15, 1216–1223. https://doi.org/10.1109/JSEN.2014.2361657.

González-Fernández, Y., Zalacain, M., Imbuluzqueta, E., Sierrasesumaga, L., Patiño-García, A., Blanco-Prieto, M.J., 2015. Lipid nanoparticles enhance the efficacy of chemotherapy in primary and metastatic human osteosarcoma cells. J. Drug Deliv. Sci. Technol. 30, 435–442. https://doi.org/10.1016/j.jddst.2015.08.004.

Hanahan, D., Weinberg, R.A., 2000. The hallmarks of cancer. Cell 100, 57–70.

Hassan, M.S.U., Ansari, J., Spooner, D., Hussain, S.A., 2010. Chemotherapy for breast cancer (Review). Oncol. Rep. 24, 1121–1131.

Hu, C.-M.J., Aryal, S., Zhang, L., 2010. Nanoparticle-assisted combination therapies for effective cancer treatment. Ther. Deliv. 1, 323–334.

Kuczynski, E.A., Sargent, D.J., Grothey, A., Kerbel, R.S., 2013. Drug rechallenge and treatment beyond progression—implications for drug resistance. Nat. Rev. Clin. Oncol. 10, 571–587. https://doi.org/10.1038/nrclinonc.2013.158.

Liu, D., Zhang, H., Fontana, F., Hirvonen, J.T., Santos, H.A., 2017. Current developments and applications of microfluidic technology toward clinical translation of nanomedicines. Adv. Drug Deliv. Rev. https://doi.org/10.1016/J.ADDR.2017.08.003.

Mao, X., Huang, T.J., 2012. Microfluidic diagnostics for the developing world. Lab Chip 12, 1412. https://doi.org/10.1039/c2lc90022j.

Matsumura, Y., Maeda, H., 1986. A new concept for macromolecular therapeutics in cancer chemotherapy: mechanism of tumoritropic accumulation of proteins and the antitumor agent smancs. Cancer Res. 46, 6387–6392.

Mitxelena-Iribarren, O., Hisey, C.L., Errazquin-Irigoyen, M., Gonzalez-Fernandez, Y., Imbuluzqueta, E., Mujika, M., Blanco-Prieto, M.J., Arana, S., 2017. Effectiveness of nanoencapsulated methotrexate against osteosarcoma cells: in vitro cytotoxicity under dynamic conditions. Biomed. Microdevices 19. https://doi.org/10.1007/s10544-017-0177-0.

Morabito, A., Carillio, G., Daniele, G., Piccirillo, M.C., Montanino, A., Costanzo, R., Sandomenico, C., Giordano, P., Normanno, N., Perrone, F., Rocco, G., Di Maio, M., 2014. Treatment of small cell lung cancer. Crit. Rev. Oncol. Hematol. 91, 257–270. https://doi.org/10.1016/J.CRITREVONC.2014.03.003.

Pandya, H.J., Dhingra, K., Prabhakar, D., Chandrasekar, V., Natarajan, S.K., Vasan, A.S., Kulkarni, A., Shafiee, H., 2017. A microfluidic platform for drug screening in a 3D cancer microenvironment. Biosens. Bioelectron. 94, 632–642. https://doi.org/10.1016/j.bios.2017.03.054.

Pathak, K., Raghuvanshi, S., 2015. Oral bioavailability: issues and solutions via nanoformulations. Clin. Pharmacokinet. 54, 325–357. https://doi.org/10.1007/s40262-015-0242-x.

Pavesi, A., Adriani, G., Tay, A., Warkiani, M.E., Yeap, W.H., Wong, S.C., Kamm, R.D., 2016. Engineering a 3D microfluidic culture platform for tumor-treating field application. Sci. Rep. 6, 26584. https://doi.org/10.1038/srep26584.

Peer, D., Karp, J.M., Hong, S., Farokhzad, O.C., Margalit, R., Langer, R., 2007. Nanocarriers as an emerging platform for cancer therapy. Nat. Nanotechnol. 2, 751–760. https://doi.org/10.1038/nnano.2007.387.

Reece, A., Xia, B., Jiang, Z., Noren, B., McBride, R., Oakey, J., 2016. Microfluidic techniques for high throughput single cell analysis. Curr. Opin. Biotechnol. 40, 90–96. https://doi.org/10.1016/J.COPBIO.2016.02.015.

Riahi, R., Tamayol, A., Shaegh, S.A.M., Ghaemmaghami, A.M., Dokmeci, M.R., Khademhosseini, A., 2015. Microfluidics for advanced drug delivery systems. Curr. Opin. Chem. Eng. 7, 101–112. https://doi.org/10.1016/j.coche.2014.12.001.

Rostami, E., Kashanian, S., Azandaryani, A.H., 2014. Preparation of solid lipid nanoparticles as drug carriers for levothyroxine sodium with in vitro drug delivery kinetic characterization. Mol. Biol. Rep. 41, 3521–3527. https://doi.org/10.1007/s11033-014-3216-4.

Sanna, V., Pala, N., Sechi, M., 2014. Targeted therapy using nanotechnology: focus on cancer. Int. J. Nanomed. 9, 467–483. https://doi.org/10.2147/IJN.S36654.

Shi, S., Han, L., Deng, L., Zhang, Y., Shen, H., Gong, T., Zhang, Z., Sun, X., 2014. Dual drugs (microRNA-34a and paclitaxel)-loaded functional solid lipid nanoparticles for synergistic cancer cell suppression. J. Control. Release 194, 228–237. https://doi.org/10.1016/j.jconrel.2014.09.005.

Soares, S., Fonte, P., Costa, A., Andrade, J., Seabra, V., Ferreira, D., Reis, S., Sarmento, B., Shi, S., Han, L., Deng, L., Zhang, Y., Shen, H., Gong, T., Zhang, Z., Sun, X., Rostami, E., Kashanian, S., Azandaryani, A.H., Dhawan, S., Kapil, R., Singh, B., Puri, A., Loomis, K., Smith, B., Lee, J.-H., Yavlovich, A., Heldman, E., Blumenthal, R., 2014. Formulation development and systematic optimization of solid lipid nanoparticles of quercetin for improved brain delivery. J. Pharm. Pharmacol. 41, 523–580. https://doi.org/10.1016/j.jconrel.2014.09.005.

Song, J., Ryu, H., Chung, M., Kim, Y., Blum, Y., Lee, S.S., Pertz, O., Jeon, N.L., 2018. Microfluidic platform for single cell analysis under dynamic spatial and temporal stimulation. Biosens. Bioelectron. 104, 58–64. https://doi.org/10.1016/J.BIOS.2017.12.038.

Stott, S.L., Hsu, C.-H., Tsukrov, D.I., Yu, M., Miyamoto, D.T., Waltman, B.A., Rothenberg, S.M., Shah, A.M., Smas, M.E., Korir, G.K., Floyd, F.P., Gilman, A.J., Lord, J.B., Winokur, D., Springer, S., Irimia, D., Nagrath, S., Sequist, L.V., Lee, R.J., Isselbacher, K.J., Maheswaran, S., Haber, D.A., Toner, M., 2010. Isolation of circulating tumor cells using a microvortex-generating herringbone-chip. Proc. Natl. Acad. Sci. USA 107, 18392–18397. https://doi.org/10.1073/pnas.1012539107.

Streets, A.M., Huang, Y., 2014. Microfluidics for biological measurements with single-molecule resolution. Curr. Opin. Biotechnol. 25, 69–77. https://doi.org/10.1016/j.copbio.2013.08.013.

Stroock, A.D., Dertinger, S.K.W., Ajdari, A., Mezic, I., Stone, H.A., Whitesides, G.M., 2002. Chaotic mixer for microchannels. Science 295, 647–651. https://doi.org/10.1126/science.1066238.

World Health Organization, 2018. Cancer (WWW Document). WHO(URL 〈http://www.who.int/cancer/en/〉)(Accessed 23 May 2018).

Yamamoto, N., Tsuchiya, H., 2013. Chemotherapy for osteosarcoma - where does it come from? What is it? Where is it going? Expert Opin. Pharmacother. 14, 2183–2193. https://doi.org/10.1517/14656566.2013.827171.

Yang, F., Teves, S.S., Kemp, C.J., Henikoff, S., 2014. Doxorubicin, DNA torsion, and chromatin dynamics. Biochim. Biophys. Acta 1845, 84–89. https://doi.org/10.1016/j.bbcan.2013.12.002.

Zuzuarregui, A., Morant-Minana, M.C., Perez-Lorenzo, E., de Tejada, G.M., Arana, S., Mujika, M., 2014. Implementation and characterization of a fully miniaturized biosensor for endotoxin detection based on electrochemical techniques. IEEE Sens. J. 14, 270–277. https://doi.org/10.1109/JSEN.2013.2282035.